LA-UR -82-2805

Conf-821037--6

LA-UR--82-2805

DE83 000609

TITLE: CALCULATIONS OF PRESSURIZED THERMAL SHOCK
PROBLEMS WITH THE SOLA-PTS METHOD

MASTER

AUTHOR(S): Bart J. Daly
Bryan A. Kashiwa
Martin D. Torrey

SUBMITTED TO: Tenth Water Reactor Safety Research
Information Meeting, Gaithersburg,
Maryland, October 12-15, 1982

Los Alamos
Los Alamos National Laboratory
Los Alamos, New Mexico 87545

DISTRIBUTION OF THIS DOCUMENT IS UNLIMITED

CALCULATIONS OF PRESSURIZED THERMAL SHOCK
PROBLEMS WITH THE SOLA-PTS METHOD

Bart J. Daly, Bryan A. Kashiwa, and Martin D. Torrey
Theoretical Division, Group T-3
University of California
Los Alamos National Laboratory
Los Alamos, NM 87545

ABSTRACT

A numerical procedure has been developed for multidimensional studies of detailed fluid-thermal mixing and wall heat transfer in the cold leg and downcomer of pressurized water reactors for application to the study of pressurized thermal shock. This method is briefly described and examples of its application to various test problems are presented to demonstrate its accuracy. An application of the method to the pressurized thermal shock problem is described for the case of a main steam line break.

I. INTRODUCTION

This report describes the SOLA-PTS computational method for fluid mixing and wall heat transfer that has been developed for application to the study of pressurized thermal shock (PTS). The conditions for PTS are a high system pressure coincident with rapid cooling of a section of vessel wall, particularly in the vicinity of neutron flux-weakened welds. The fluid dynamics problem is to predict the temperature of the vessel wall for a variety of different accident scenarios.

These accident sequences can be subdivided into two main classes: those with and those without loop flow. When loop flow is maintained, the transient solution is obtained by a systems code analysis. While these codes may be able to predict the system response to a particular accident scenario quite accurately, they cannot provide detailed information about the thermal distribution along

the vessel wall. It is the purpose of the numerical method described here to provide that detailed information for those accident scenarios where it is suspected that there is incomplete mixing in the downcomer, and for isolated times during a transient. This is accomplished by taking the systems code data at a particular location in the cold leg as input boundary conditions for the detailed calculations. Holding these boundary conditions fixed in time, a three-dimensional **steady state** solution is computed showing the flow field and thermal distribution in the cold leg and downcomer. The walls are generally treated adiabatically in order to hasten the approach to steady state. The steady state fluid temperature distribution adjacent to the vessel wall can then be used to conservatively estimate the temperature distribution in the metal. The use of the adiabatic wall treatment in this case is justified because the effect of wall heat transfer should be small compared to the heat exchange that results from the mixing of the emergency core coolant (ECC) water with the loop flow. If the adiabatic treatment indicates that conditions for crack initiation are present, then the inclusion of wall heat flux to avoid crack initiation cannot be conservatively justified since the fracture mechanics aspects of the problem are not well enough known.

The results of these three-dimensional calculations do not influence the system code solution, because the details of the downcomer flow have little effect on the loop flow calculation. Regardless of what fluid motions develop in the downcomer, the fluid should be throughly mixed in the lower plenum region.

The second main class of problems, those without loop flow, do not require a system code solution. The requirement in this case is to calculate the **transient**

mixing of ECC water with the stagnant (or rapidly decelerating) hot water in the cold leg, downcomer and lower plenum. In this case wall heat transfer is included in the calculations, since for this problem it is the rate at which the wall temperature cools that will determine the probability for crack initiation.

Section II of this paper provides a description of the numerical method. Some calculational examples that were used to test the code are described in this section. Section III provides the results of an application to a PTS problems, and concluding remarks are made in Sec. IV.

II. THE COMPUTATIONAL MODEL

The SOLA-PTS code had its origen in the SOLA[1] and SOLA-VOF[2] codes developed at Los Alamos. It is a computational model for the solution of transient, incompressible, single-phase flow problems, together with wall heat transfer and thermal transport. The code exists in both two- and three-dimensional forms. The two-dimensional code is used for testing models and for scoping studies, while the three-dimensional code is applied to the solution of detailed PTS problems.

Using the original solution algorithm incorporated in the SOLA codes, the following equations are solved in SOLA-PTS*

$$\frac{\partial u_i}{\partial x_i} = 0 \tag{1}$$

$$\frac{\partial u_i}{\partial t} + u_j \frac{\partial u_i}{\partial x_j} = -\frac{1}{\rho} \frac{\partial p}{\partial x_i} + \frac{\partial \tau_{ij}}{\partial x_j} + [1 - \beta(T - T_0)]g_i \tag{2}$$

$$\frac{\partial T}{\partial t} + u_i \frac{\partial T}{\partial x_i} = \frac{\partial}{\partial x_i} \left(\sigma_f \frac{\partial T}{\partial x_i} \right) \tag{3}$$

---

*The definition of the variables is provided in the nomenclature.

$$\frac{\partial T}{\partial t} = \frac{\partial}{\partial x_i} \left(\sigma_m \frac{\partial T}{\partial x_i} \right) \tag{4}$$

Equations (1) - (3) are solved in the fluid, and Eq. (4) is solved in the metal. Note that Eqs. (2) and (3) are in non-conservative form. This form is used instead of the conservative form because of a zero-order truncation error that results with the use of the latter in conjunction with a variable computacional mesh. In order to optimize computing efficiency, it is essential to utilize a scheme that maintains good accuracy with a variable grid. Hence conservative schemes are unacceptable for these PTS studies.

To ensure a stable, accurate solution to the above equations we make use of the Tensor Viscosity method[3] for the calculation of spatial derivatives, together with the Filtering Remedy and Methodology (FRAM) method[4] for the suppression of dispersion errors. The Tensor Viscosity method is the multidimensional analog of one-dimensional, interpolated donor cell. It is a second-order-accurate difference scheme that is formulated by evaluating the convective terms using forward-time, space-centered derivatives, and then modifying the equations by the addition of a term,

$$- \frac{1}{2} \, \delta t \, \frac{\partial}{\partial x_i} \left(u_i u_j \frac{\partial \phi}{\partial x_j} \right) \ ,$$

to the right side of the equation. Here ϕ represents the temperature or a velocity component.

As with any second order method, the Tensor Viscosity method can suffer from dispersion errors when used without some type of filtering procedure, such as FRAM. In the FRAM method, a provisional estimate for the value of a variable at

an advanced time level is made using any given high-order differencing technique. The provisional value is compared to the maximum and minimum of the advanced time values obtained by neglecting convection at the computational cell in question and its four adjacent neighbors. If the provisional, high-order value falls between the maximum and minimum, it is considered to be the advanced time solution; if not, it is replaced by a solution based on a low-order, diffusive differencing technique. In all of the studies that follow, full upwind differencing is used as the low-order technique. An alternative procedure would be to replace the provisional solution by the maximum or minimum value, whichever is exceeded. However, this procedure has not yet been tested.

Dukowicz and Ramshaw[3] tested the accuracy of the Tensor Viscosity method by examining the diffusion of a step function transported with a constant velocity. In this test the scalar transport equation

$$\frac{\partial \phi}{\partial t} + u \frac{\partial \phi}{\partial x} + v \frac{\partial \phi}{\partial y} = 0 \tag{5}$$

is solved in a square computational space with $\delta x = \delta y = 1.0$, $u = v = 1.0$ and $\delta t = 0.2$. The initial value of ϕ in the space is 1.0, and a value 2.0 is specified at the bottom and left inflow boundaries. The right and top boundaries had a continuative outflow specification. We have repeated this test for the Tensor Viscosity method and for two other second-order methods, Leith's method[5] and Crowley's method,[6] all in conjunction with FRAM. Results of these calculations, showing the appearance of the step function at times of 0.4 and 0.8, are presented in Fig. 1. The Tensor Viscosity method shows the least effects of numerical diffusion. As a measure of the differences, one can compare the increase in

the distance from the high contour line to the low contour line between the two times plotted in Fig. 1. For the Leith method this increase is 26%; for the Crowley method the increase is 23%; for the Tensor Viscosity method the increase is 17%.

The SOLA-PTS code was also tested by computing the development of the laminar thermal boundary layer in the presence of the developing hydrodynamic boundary layer between parallel planes. The solution to this problem for non-buoyant flows is available and has been verified by experiment.[7]

Figures 2 through 6 illustrate the results of the SOLA-PTS calculation of the parallel plane thermal-hydrodynamic entry length problem with a constant heat flux at one plane and zero heat flux at the other. In this study Pr = 0.7 and Re = 40. Figures 4 through 6 show comparison of SOLA-PTS results (solid line) to the analytic solution of Heaton et al.[7] (marked by A's). These figures show excellent comparison despite having only ten computing zones across the channel in the SOLA-PTS calculation. As expected, the only significant deviation from the analytic solution occurs very near the entrance where there is a significant v component to the velocity.

The two-equation k-ε turbulence model of Launder and Spalding[8] has been included in the SOLA-PTS code. The only modification to the equations presented in Ref. 8 has been the addition of a set of terms reflecting the alteration in turbulence energy and decay rate due to buoyancy. The equations as they are currently employed in this eddy diffusivity method are

turbulence viscosity:

$$\nu_t = \frac{C_\mu k^2}{\epsilon} \quad , \tag{6}$$

turbulence energy:

$$\frac{Dk}{Dt} = \frac{\partial}{\partial x_j}\left[\left(\frac{\nu_t}{\sigma_k} + \nu_o\right)\frac{\partial k}{\partial x_j}\right] + \nu_t\left[\frac{\partial u_i}{\partial x_j}\left(\frac{\partial u_i}{\partial x_j} + \frac{\partial u_j}{\partial x_i}\right) + \beta g_i\frac{\partial T}{\partial x_i}\right] - \epsilon \quad , \qquad (7)$$

turbulence decay rate:

$$\frac{D\epsilon}{Dt} = \frac{\partial}{\partial x_j}\left[\left(\frac{\nu_t}{\sigma_\epsilon} + \nu_o\right)\frac{\partial \epsilon}{\partial x_j}\right] + C_1\frac{\epsilon}{k}\nu_t\left[\frac{\partial u_i}{\partial x_j}\left(\frac{\partial u_i}{\partial x_j} + \frac{\partial u_j}{\partial x_i}\right) + \beta g_i\frac{\partial T}{\partial x_i}\right] - C_2\frac{\epsilon^2}{k} \quad , \quad (8)$$

turbulence decay rate near the wall:

$$\int_0^{y_p} \epsilon\, dy = \frac{C_\mu}{\kappa}k_p^{3/2}\,\ell n\left[\frac{E\, y_p(C_\mu^{\frac{1}{4}}k_p)^{\frac{1}{2}}}{\nu_o}\right] \quad , \qquad (9)$$

wall shear stress:

$$\frac{u_p(C_\mu^{\frac{1}{4}}k_p)^{\frac{1}{2}}}{(\tau/\rho)_w} = \frac{1}{\kappa}\,\ell n\left[\frac{E\, y_p(C_\mu^{\frac{1}{4}}k_p)^{\frac{1}{2}}}{\nu_o}\right] \quad . \qquad (10)$$

wall heat flux:

$$\frac{(T_p - T_w)c_p\rho(C_\mu^{\frac{1}{4}}k_p)^{\frac{1}{2}}}{\dot{q}_w''} = \frac{\sigma_h}{\kappa}\,\ell n\left[\frac{E\, y_p(C_\mu^{\frac{1}{4}}k_p)^{\frac{1}{2}}}{\nu_o}\right]$$

$$+ \sigma_h\frac{\pi/4}{\sin(\pi/4)}\left(\frac{A}{\kappa}\right)^{\frac{1}{2}}\left(\frac{Pr}{\sigma_h} - 1\right)\left(\frac{\sigma_h}{Pr}\right)^{1/4} \qquad (11)$$

The equation for wall shear stress Eq. (10) is used to account for the effect of wall drag in the PTS calculations. The wall shear stress is also used to esti-

mate the velocity gradient outside the laminar sublayer for the calculation of the shear creation terms in Eqs. (7) and (8).

The turbulence model embodied in Eqs. (6) through (11) has been extensively studied for a wide range of experimental data.[8] We have applied the model as it is included in the SOLA-PTS code to the study of turbulent flow between parallel planes. A comparison of these calculated results with Laufer's[9] experimental data for fully developed flow between parallel planes is given in Fig. 7. In this study the velocity and turbulence energy profiles are plotted versus posi- tion in the channel of half-spacing d. The computed values, given by the symbols in Fig. 7, were obtained from a one-dimensional channel flow calculation with $Re = 61,600$ and $\nu_o = 0.002$ cm^2/s using a specified pressure gradient. In this way, ν is a function of y alone. Three calculations were performed to test the sensitivity of results to the finite difference resolution. It is clear from Fig. 7 that the results are not sensitive to mesh size and that good agreement is achieved even when there are only five computational zones across the channel width.

III. PTS CALCULATION

As an example of a PTS application we present results obtained in SOLA-PTS calculations of a main steam line break (MSLB) transient, using data from a TRAC system code calculation as our input conditions. We chose to perform the calcu- lation at a time of 160 s into the transient, when the pressure is at 50 bars, the pumps have coasted down, and there is no vent valve flow into the downcomer. At this time the thermal-hydraulics are characterized by a high temperature (> 500 K), low velocity flow in the intact loops, and a low temperature (< 420 K), high velocity flow in the broken loop. The high velocity flow on the

broken loop side is driven by natural convection as a result of the large temperature difference between the upper plenum and the steam generator on that loop. The input conditions for these calculations are shown in Table I.

Figures 8-11 show results obtained in the broken loop calculation. Figures 8-9 are velocity vector plots in the horizontal plane at the elevation of the ECC injection and in the vertical plane through the centerline of the cold leg, respectively. In this calculation the loop flow is injected into the cold leg at a position 8.4 m upstream from the entrance to the downcomer and the coolant enters the cold leg 5.6 m upstream. Both plots show that as the fluid enters the downcomer it splashes against the core barrel wall, while the flow region adjacent to the vessel wall is relatively stagnant. The non-fluid region in the bottom left corner of Fig. 8 is the hot leg obstruction. Note the variable mesh in this calculation, with fine noding in the region of the ECC injection.

The velocity plot in Fig. 10 shows the flow development in the plane adjacent to the vessel wall. These fluid motions result primarily from recirculation of the main flow, which lies adjacent to the core barrel. The expanding flow in the top center of the plot is the cold leg inflow. The hot leg is at the upper left.

The temperature distribution adjacent to the vessel wall is shown in the contour plot of Fig. 11. The minimum temperature is at the cold leg inlet, where the fluid is approximately 10°C cooler than the average fluid temperature in this plane. However, even this coldest fluid has a temperature of 407 K, indicating that there has been thorough mixing of the 303.3 K ECC water (see Table I) with the loop flow in the cold leg. Thus, at this time in the transient there appears to be no threat of crack initiation in the vessel wall on the broken loop side.

Figures 12-15 show results obtained in the intact loop calculation. The velocity vectors in the horizontal and vertical planes corresponding to those of Figs. 8 and 9 are not shown. They appear very similar to Figs. 3 and 9 except that, because of the reduced loop flow in the present calculation, the ECC injection exerts a greater influence on the cold leg flow. Figures 12 and 13 show velocity vector plots in the planes adjacent to the core barrel and vessel walls. These plots demonstrate the coherent flow pattern adjacent to the core barrel (Fig. 12), resulting from the impact of cold leg flow, and the lack of coherent flow adjacent to the vessel wall, corresponding to relatively stagnant flow conditions. These stagnant conditions adjacent to the vessel wall are also evident in the temperature contour plot in that plane, shown in Fig. 14. With the exception of a relatively cold region near the cold leg inlet, the temperatures are practically uniform throughout this plane. The minimum temperature here is 514 K, which indicates no threat to the integrity of the vessel wall at this time in the transient.

Figure 15 shows the temperature contour plot in a vertical plane containing the cold leg centerline. The effect of the ECC injection at the cold leg boundary is evident in this centerline plot, but the temperature variation from upstream values is minor. Note that a stratified flow condition persists to the downcomer.

IV. SUMMARY

A brief description has been presented of the SOLA-PTS computational method for multidimensional calculation of fluid-thermal mixing and wall heat transfer, with particular application to the study of pressurized thermal shock. Several computational examples have been presented to demonstrate the accuracy of the computational algorithm and the turbulence model employed.

This method will be applied to two classes of computational problems that arise in the pressurized thermal shock study. The first of these is the problem of calculating the mixing of ECC water with loop flow, with or without vent valve flow, in the cold leg and downcomer in order to determine the fluid temperature distribution along the vessel wall. These problems are calculated as steady-state solutions, using systems code information to provide the inlet boundary conditions, in order to provide, "snapshots" of the thermal distributions at isolated times during a transient. An example of results obtained in a main steam line break transient have been presented as illustration of this procedure.

The second application of the SOLA-PTS method has been to the transient calculation of fluid-thermal mixing and wall heat transfer in the cold leg and downcomer when there is no loop flow in the system. In this case the temperature throughout the downcomer will eventually reach the ECC temperature. The objective is to calculate the rate of cooling of the metal in the vessel wall. Calculations of this type are being persued at the present time.

REFERENCES

1. C. W. Hirt, B. D. Nichols, and N. C. Romero, "SOLA - A Numerical Solution Algorithm for Transient Fluid Flows," Los Alamos Scientific Laboratory report LA-5852, April 1975.

2. B. D. Nichols, C. W. Hirt, and R. S. Hotchkiss, "SOLA-VOF: A Solution Algorithm for Transient Fluid Flow with Multiple Free Boundaries," Los Alamos Scientific Laboratory report LA-8355, August 1980.

3. J. K. Dukowicz and J. D. Ramshaw, "Tensor Viscosity Method for Convection in Numerical Fluid Dynamics," J. Comput. Phys. 32, 71-79 (July 1979).

4. M. Chapman, "FRAM: Nonlinear Damping Algorithms for the Continuity Equation," J. Comput. Phys. 44, 84-103 (1981).

5. P. J. Roache, Computational Fluid Dynamics, Hermosa Publishers, Albuquerque, NM (1972).

6. W. P. Crowley, "Second-Order Numerical Advection," J. Comput. Phys. 1, 471-484 (1967).

7. H. S. Heaton, W. C. Reynolds, and W. M. Kays, "Heat Transfer in Annular Passages. Simultaneous Development of Velocity and Temperature Fields in Laminar Flow," Int. J. Heat Mass Transfer 7, 763-781 (1964).

8. B. E. Launder and D. B. Spalding, "The Numerical Computation of Turbulent Flows," Comput. Meth. in App. Mech. and Eng. 3, 269-289 (1974).

9. J. Laufer, "Investigation of Turbulent Flow in a Two-Dimensional Channel," NACA Report 1053 (1951).

TABLE I

INPUT CONDITIONS, MAIN STEAM LINE BREAK

	Velocity (cm/s)	Temperature (K)	Area (cm^2)	Flow Rate (cm^3/s)
Broken Loop				
ECC	175.83	303.3	77.4	1.361×10^4
Loop	149.64	418.0	3969.0	5.939×10^5
Intact Loop				
ECC	125.6	303.3	108.4	1.361×10^4
Loop	40.1	527.9	3969.0	1.592×10^5

Nomenclature

Symbols

c_p	Specific heat
D_h	Hydraulic diameter
H	Plate spacing
k	Turbulence energy
p	Pressure
Pr	Prandtl number
$\dot{q}_w''$	Heat flux
Re	Reynolds number
t	Time
T	Temperature
u_i	Velocity component in i direction
x_i	Spatial coordinate i
y	Distance

Greek Symbols

β	Fluid volume coefficient of expansion
δt	Time increment
ε	Turbulence energy decay rate
ν	Kinematic viscosity
ρ	Fluid density
σ	Thermal diffusivity
τ	Shear stress
ϕ	Velocity component or scalar

Subscripts

e   Entrance

f   Fluid

i   Insulated

m   Metal

o   Reference or molecular value

p   Value at center of fluid cell adjacent to wall

t   Turbulent

w   Wall

Constants

A   Van Driest's constant (26.0)

C_1 1.44

C_2 1.92

C_μ 0.09

E   9.0

g_i Gravitational acceleration in i direction

κ 0.4

σ_h Turbulent Prandtl number (assumed 1.0)

σ_k 1.0

σ_ε 1.3
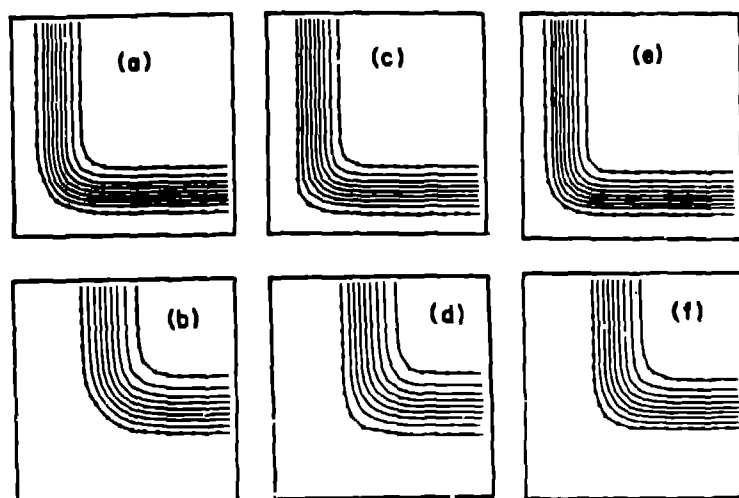
Fig. 1. Contours of ϕ for Leith's method at t = 0.4 (a) and t = 0.8 (b), Crowley's method at t = 0.4 (c) and t = 0.8 (d), and the Tensor Viscosity method at t = 0.4 (e) and t = 0.8 (f). The three methods are used in conjunction with the FRAM procedure (see text).

Fig. 2. Temperature contours for the laminar thermal-hydraulic entry length for parallel planes, one plane with constant heat flux and the other plane insulated. The incoming temperature is 400 K, $\dot{q}_w''/\rho c_p$ = 31.49 cm K/s, the plate spacing H is 10.0 cm, the Reynolds number Re based on mean velocity and hydraulic diameter D_h is 40, and the Prandtl number Pr is 0.7. The high contour (H) is 898.2 K and the low contour (L) is 455.4 K.
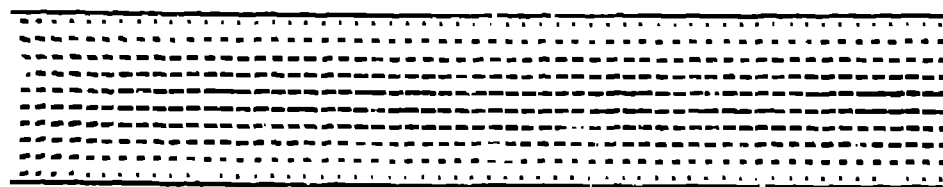
Fig. 3. Velocity vectors for the laminar th mal-hydrodynamic entry length problem, showing the developing velocity profile.

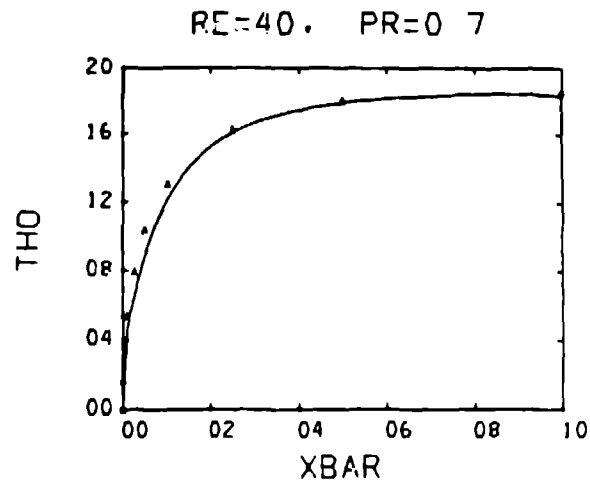## RE=40, PR=0 7

RE=40, PR=0 7
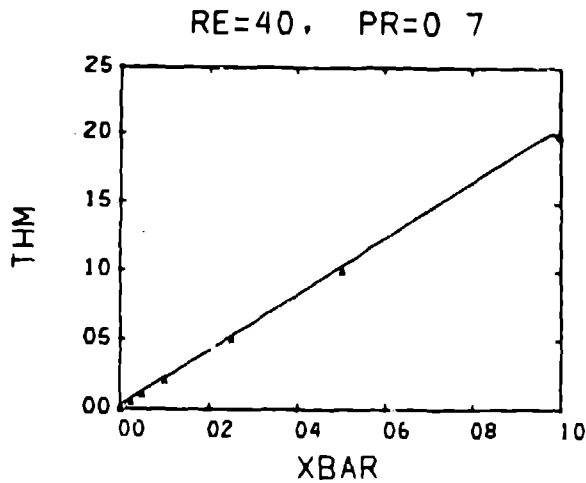
Fig. 4. Non-dimensional mean temperature THM vs non-dimensional distance XBAR for the laminar thermal-hydrodynamic entry length problem. $XBAR \equiv x/(D_h RePr)$,

$$THM \equiv (\overline{T} - T_e) \frac{\sigma_f \rho c_p}{\dot{q}_w'' D_h},$$

where $\overline{T} \equiv \int_o^H uT \, dy / \int_o^H u \, dy.$

Fig. 5. Non-dimensional heated wall temperature THO vs non-dimensional distance for the laminar thermal-hydrodynamic entry length problem.

$$THO = (T_w - \overline{T}) \frac{\sigma_f \rho c_p}{\dot{q}_w'' D_h}.$$

RE=40, PR=0 7

Fig. 6. Non-dimensional insulated wall temperature THI vs non-dimensional distance for the laminar thermal-hydrodynamic entry length problem.

$$THI \equiv (T_1 - \overline{T}) \frac{\sigma_f \rho c_p}{\dot{q}_w'' D_h}.$$
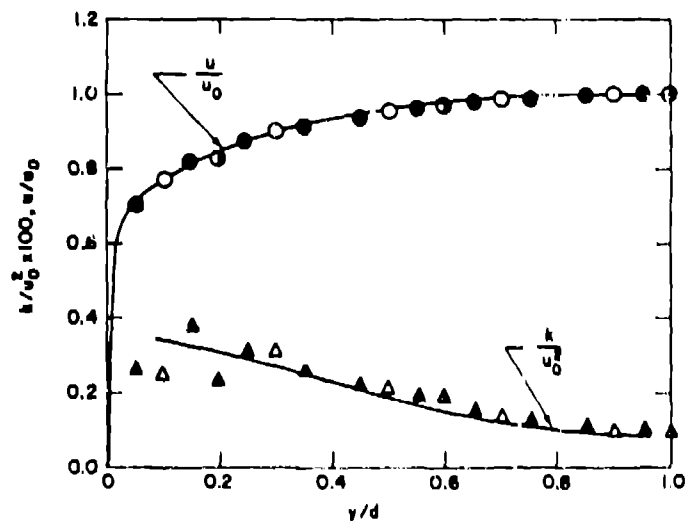
Fig. 7. Turbulence velocity and turbulence energy profiles for flow between parallel planes at Re = 61,600. The solid line is from the experimental data of Laufer (Ref. 9), the solid symbols are from a one dimensional SOLA-PTS calculation with 20 cells across the channel, the open symbols are from a calculation with 10 cells across the channel, and the half-opened symbols are from a calculation with 5 cells across the channel.
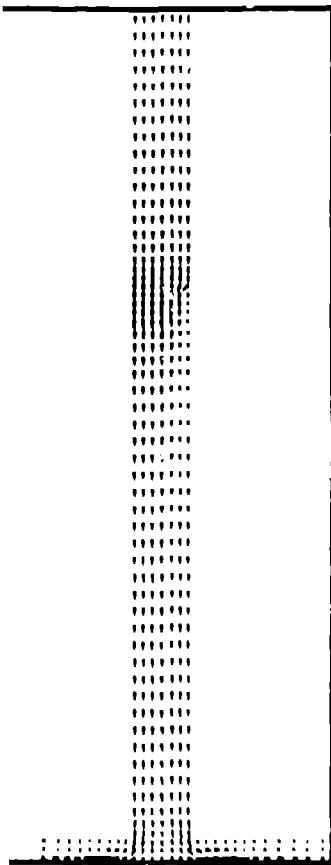
Fig. 9. Velocity vector plots in the vertical plane through the cold leg centerline for the broken loop calculation at 160 s into the MSLB transient. The cold leg flow impacts the core barrel wall at the left.

Fig. 8. Velocity vector plots in the horizontal plane at the
(see elevation of the ECC injection for the broken loop
left) calculation at 160 s into the MSLB transient. The cross-flow vectors in the cold leg show the FCC injection. The downcomer is located at the bottom of the plot and the hot leg obstruction is in the bottom left corner.
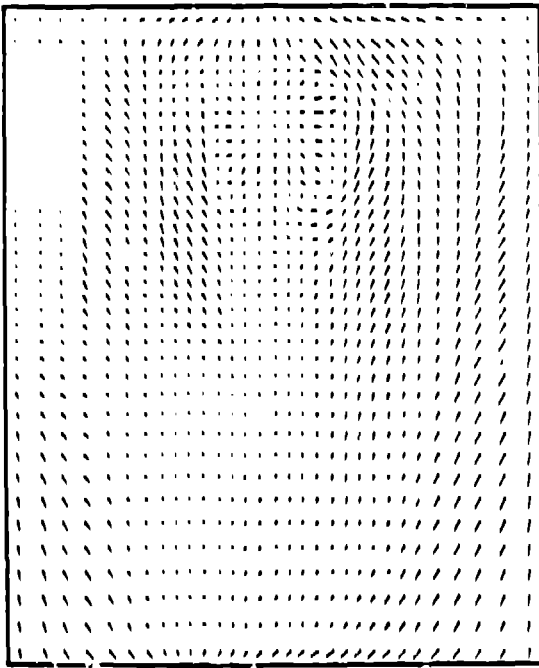
Fig. 10. Velocity vector plot in the plane adjacent to the vessel wall for the broken loop calculation at 160 s into the MSLB transient. The expanding flow in the upper center of the plot is the cold leg inflow. The hot leg obstruction is at the upper left.
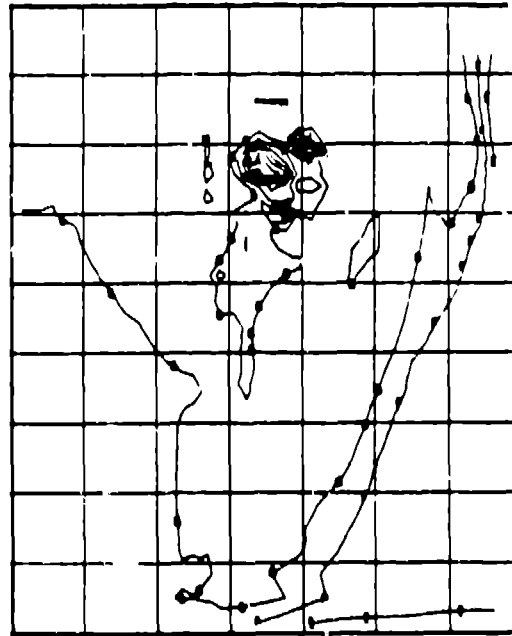
Fig. 11. Temperature contour plot in the plane adjacent to the vessel wall for the broken loop calculation at 160 s into the MSLB transient. The minimum contour (A) has the value 407.1 K and the contour interval is 1.57 K.
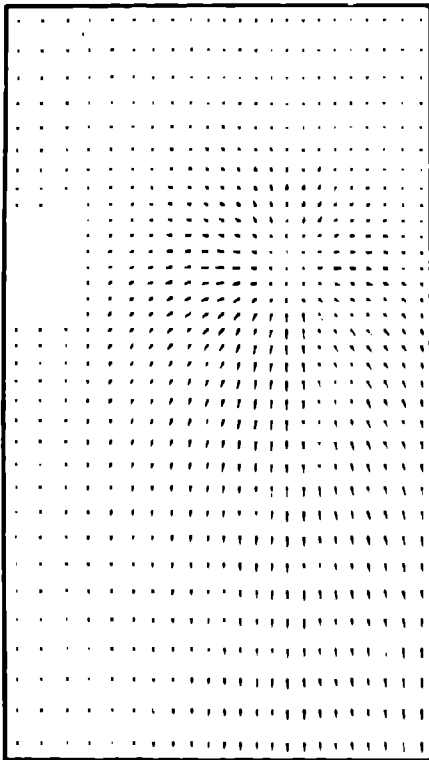
Fig. 12. Velocity vector plot in the plane adjacent to the core barrel wall for the intact loop calculation at 160 s into the MSLB transient. A greater part of the upper downcomer region is included here than in the broken loop calculation.
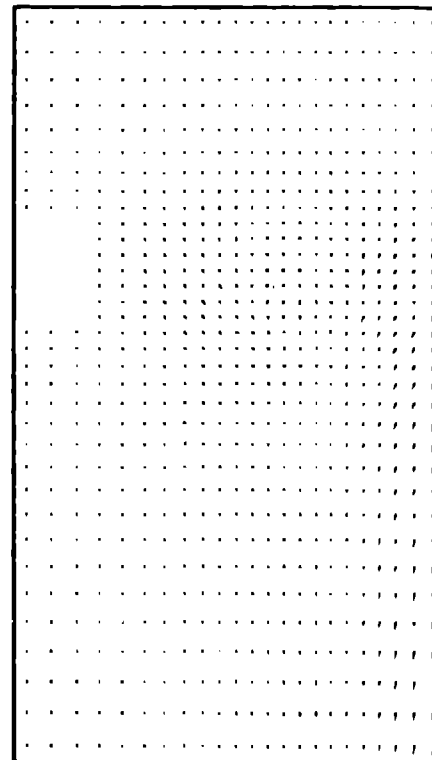
Fig. 13. Velocity vector plot in the plane adjacent to the vessel wall for the intact loop calculation at 160 s into the MSLB transient.
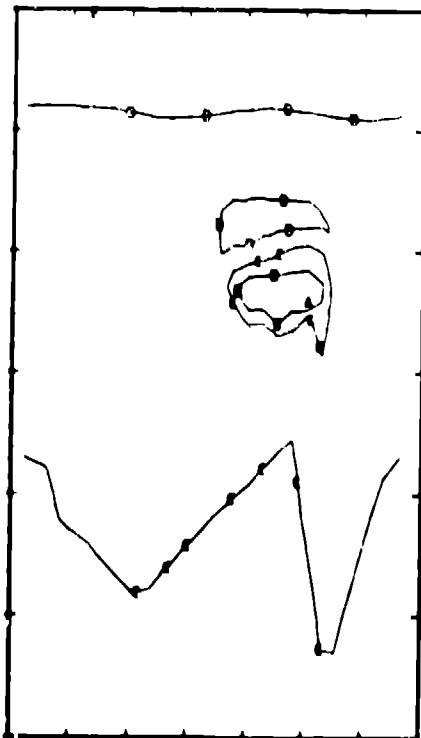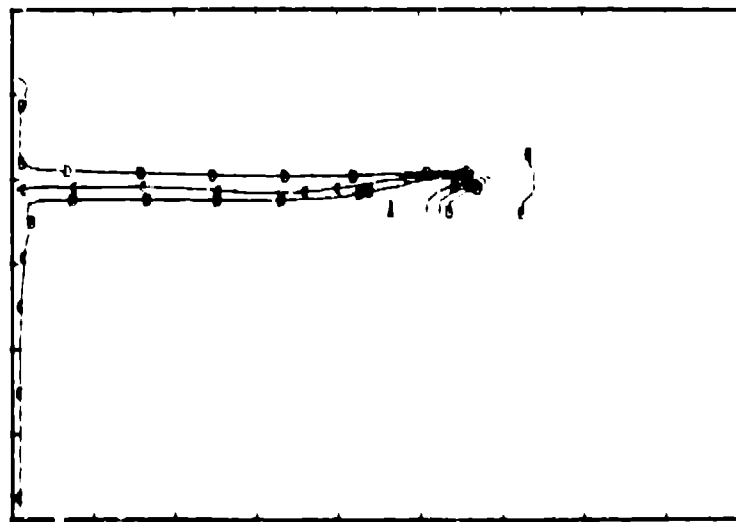

Fig. 15. Temperature contour plot in a vertical plane through the cold leg centerline for the intact loop calculation at 160 s into the MSLB transient. The minimum contour (A) is 510.9 K and the contour interval is 4.25 K.

Fig. 14. Temperature contour plot in the plane adjacent to (see the vessel wall for the intact loop calculation at left) 160 s into the MSLB transient. The minimum contour (A) is 514.2 K and the contour interval is 3.41 K.